JOURNAL OF SOLID STATE CHEMISTRY 4, 173–185 (1972)

Crystallographic Shear in $WO_3 \cdot xNb_2O_5$ ($x = 0.03$–0.09)

J. G. ALLPRESS

Division of Tribophysics, C.S.I.R.O., University of Melbourne, Parkville, Victoria 3052, Australia

Received May 10, 1971

Tungsten trioxide samples doped with 3–9 mole% of niobium pentoxide have been examined by electron diffraction and microscopy. The effect of the dopant is to introduce crystallographic shear (CS) planes, which lie parallel to $\{100\}_R$, $\{410\}_R$, and $\{210\}_R$ (R = ReO_3-type parent lattice), depending upon the composition. Idealized models for these CS structures are suggested, and the results are discussed in terms of the relative stability of various possible structures, and the formation and diffusion of CS surfaces.

1. Introduction

The accommodation of nonstoichiometry by means of crystallographic shear planes (CS) in compounds which are structurally related to ReO_3 has been thoroughly established by means of X-ray studies of comparatively well-ordered single crystals (*1*, *2*). However, many materials of this kind are difficult, if not impossible to prepare in an ordered state, and in these cases, X-ray techniques are of limited value. The recent applications of electron microscopy to these systems (*3–6*) has shown that the CS planes can be observed directly, and their arrangement, whether random or ordered, can be determined.

The structure of WO_{3-x} for $x \leqslant 0.05$ serves as an example of the information which can be derived by these means. The structure of ordered $W_{20}O_{58}$ (*7*), which was determined by X-ray methods, contains CS planes parallel to $\{310\}_R$ (R = ReO_3-type parent structure), regularly arranged with a spacing of 23.3 Å. Disordered arrangements of CS planes in the same direction have been observed by electron microscopy in nonequilibrium samples of $WO_{\sim 2.90}$ (*6*). At compositions closer to stoichiometry ($x \leqslant$ *ca.* 0.02), the CS planes lie parallel to $\{210\}_R$, and are more or less randomly spaced (*5*, *8*). Even for $x = 0.0001$, isolated defects of this type have been observed (*8*), indicating that the concentration of point defects (vacant oxygen sites) is probably very low, and does not contribute significantly to the observed wide range of composition in WO_{3-x}.

Apart from reduction of W^{6+} to W^{5+}, a second means of varying the oxygen/metal ratio in WO_{3-x} is to introduce cations of lower valency, such as Nb^{5+}. There have been several accounts of X-ray work on WO_3 containing small additions of Nb_2O_5 and Ta_2O_5. Roth and Waring (*9*) studied the Nb_2O_5–WO_3 phase diagram and found evidence for at least two phases containing 6–9 mole% of Nb_2O_5. They were unable to determine their exact compositions, but their powder diffraction patterns showed similarities with those of the WO_{3-x} phases. At still lower concentrations of Nb_2O_5 (2–3 mole%), they observed phases which were closely related to several of the polymorphs of WO_3. Gadó and Magnéli (*10*) made similar observations using Nb_2O_5 and Ta_2O_5 as dopants.

The present paper describes some electron microscope observations on the CS structures of WO_3 containing 3–9 mole% of Nb_2O_5. They were made following similar studies of WO_{3-x} (*6*, *8*), in order to compare the direction and arrangement of CS planes associated with doping, with those produced during reduction of WO_3.

2. Experimental

Most of the samples were kindly provided by Dr. R. S. Roth, and were taken from batches prepared at the U.S. National Bureau of Standards during a phase study of the Nb_2O_5–WO_3 system (*9*). They were prepared from high-purity starting materials, by heating the component oxides together in sealed platinum capsules, initially at 1473°K for 2 hr, then for longer periods at temperatures up to 1623°K, and finally quenching the capsules into water. The

TABLE I

Molar composition $Nb_2O_5:WO_3$	Final heat treatment Temp (°K)	Time (hr)	Number of fragments containing CS planes parallel to $\{100\}_R$	$\{410\}_R$	$\{210\}_R$
1:11	1552	65	10	—	—
	1584	70	12	—	—
	1623	17	8	2	—
1:11.5	1574	69	10	—	—
1:12	1584	70	10	1	—
1:13	1584	70	8	2	1
1:14	1585	68	7	3	1
1:15	1552	65	6	4	—
	1585	68	2	9	—
	1623	17	1	14	6
1:15.7	1572	67	5	5	1
1:24[a]	1574	68	—	1	3
	1628	19	—	—	6
1:32.3[a]	1628	19	—	—	4

[a] The majority of fragments in these samples did not contain CS planes—their diffraction patterns correspond to one or other of the forms of WO_3, stabilized by the presence of small amounts of Nb_2O_5 in solid solution (*9*).

compositions and final heat treatments of the samples are recorded in Table I.

Specimens suitable for electron microscopy were obtained by grinding the samples in an agate mortar and dispersing some of the fine powder on carbon-coated grids. A small proportion of the resulting fractured fragments were sufficiently thin for examination by electron diffraction and microscopy at 100 kV. A double tilting specimen stage was used, so that specific orientations of individual fragments could be obtained.

3. Results

3.1 Electron Diffraction

In order to assess the homogeneity of the samples, at least ten fragments in each were examined by electron diffraction. Patterns containing streaked reflections or superlattice spots additional to those expected from a subcell of WO_3 were sought, and three distinct types, shown in Fig. 1 were found. In each of these, there is a square array of strong spots, typical of the pseudocubic ReO_3-type lattice of WO_3. Some of these spots are labelled with indices appropriate to this sublattice. In addition, this array is traversed by streaked lines which lie parallel to the $(100)_R$, $(410)_R$, and $(210)_R$ reciprocal sublattice directions in Figs. 1a–b, c, and d, respectively. The incidence of these three patterns among the samples varied with composition as shown in Table I. Streaking parallel to $(100)_R$ predominated at higher concentrations of Nb_2O_5 (1:11–1:14). As the Nb_2O_5 content was reduced to 1:15, streaking parallel to $(410)_R$ was found more frequently and

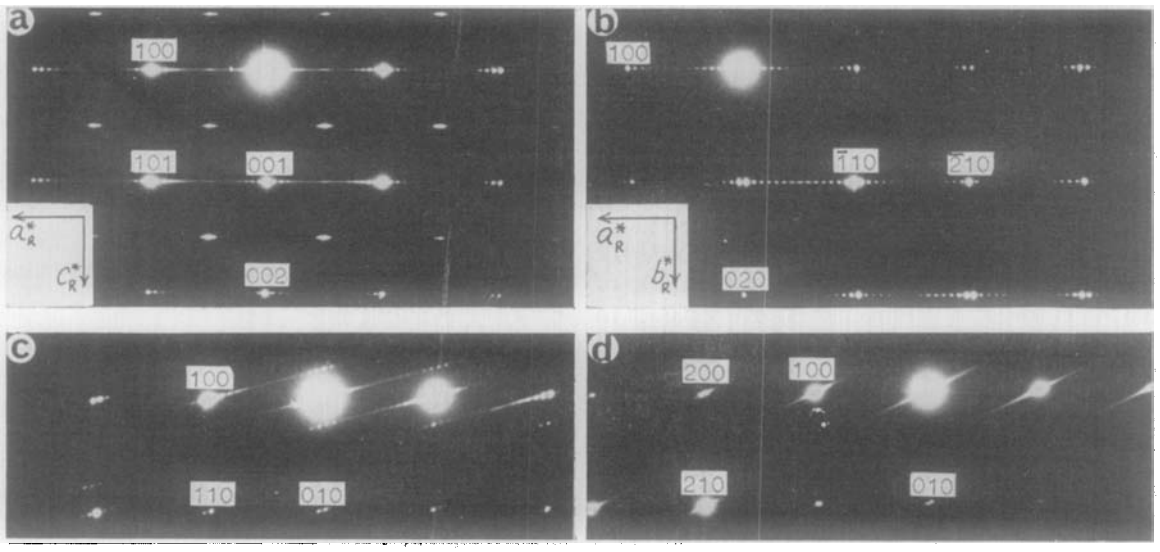

FIG. 1. Electron diffraction patterns from fragments of $WO_3 \cdot xNb_2O_5$. The strongest spots in each pattern lie in a square array, indexed in terms of a ReO_3-type subcell, to which the axes a_R^*, b_R^*, and c_R^* refer. The patterns contain extra spots and streaks in lines parallel to $(100)_R$ in (a–b), $(410)_R$ in (c), and $(210)_R$ in (d). The spot intensities are not symmetrical about 000, because the incident electron beam was not exactly parallel to the zone axes. The fragments were taken from samples of nominal composition $Nb_2O_5:WO_3$ = 1:11 (a), 1:12 (b), 1:15.7 (c), and 1:15 (d).

appeared to be favored by higher temperatures of preparation. The 1:15 sample prepared at the highest temperature (1623°K) contained a significant proportion of fragments whose patterns were streaked parallel to $(210)_R$. Fragments of this type were also found at much lower Nb_2O_5 concentrations (1:24, 1:32.3). At these compositions, the samples also contained one or other of the forms of WO_3, stabilized by the presence of small amounts of Nb_2O_5 in solid solution (*9*). Occasionally, patterns contained streaks in several directions, e.g., parallel to $(100)_R$ and $(410)_R$; $(410)_R$ and $(4\bar{1}0)_R$; $(120)_R$, $(1\bar{2}0)_R$, $(210)_R$, and $(2\bar{1}0)_R$.

Roth and Waring concluded from their X-ray observations (*9*) that two phases were present in this composition region, having Nb_2O_5:WO_3 molar ratios close to 1:11 and 1:15. The present examination indicates that these two phases are most probably those in which the superlattice spots and streaks in the diffraction patterns lie parallel to $(100)_R$ and $(410)_R$, respectively. The presence of minor amounts of a third phase giving patterns containing streaks parallel to $(210)_R$ would be very difficult to detect by X-ray powder techniques.

The "spottiness" of the streaks in the patterns varied widely between fragments, and the patterns in Fig. 1 were chosen to show the spots most clearly. The $(210)_R$ patterns were always heavily streaked (Fig. 1d), but the others frequently contained well-resolved superlattice spots, particularly in the vicinity of the sublattice reflections.

The $(100)_R$ patterns (Fig. 1a–b) contained spots which subdivided the a_R^* axis of the reciprocal sublattice into either 14, 15, or 16 parts. The degree of subdivision was most commonly 14, and tended to increase to 15 and 16 as the Nb_2O_5 content of the samples was reduced. However, none of the samples was completely homogeneous from this point of view. A close inspection of the *hk*0 sections (e.g., Fig. 1b) showed that the allowed reflections all had $(h + k)$ even. The *h*0*l* sections were more complex, in that the c_R^* axis of the subcell was halved (e.g., Fig. 1a). The strongest reflections in both these sections form patterns which are very similar to those of the tetragonal high temperature form of WO_3, and of the solid solution $3Nb_2O_5 \cdot 97WO_3$ (*9*), which has the unit cell dimensions $a = 5.265$ Å ($\simeq 3.7\sqrt{2}$), $c = 3.846$ Å. The approximate dimensions of the orthorhombic supercell, derived from patterns such as Fig. 1a, b, are

$$a = 2n \times 3.70\,\text{Å}, \qquad b = 3.72\,\text{Å}, \qquad c = 2 \times 3.85\,\text{Å},$$

where n is the subdivision of the a^* axis = 14, 15, or 16. With this result as a basis, the unindexed X-ray powder data given by Roth and Waring (*9*) for $Nb_2O_5 \cdot 11WO_3$ were examined. Table II lists a possible indexing, using a unit cell of dimensions

$$a = 103.3\,\text{Å (i.e., } n = 14), \qquad b = 3.729\,\text{Å}, \qquad c = 3.852\,\text{Å}.$$

Most of the lines in the pattern were capable of being indexed by several combinations of h, k, and l and Table II contains only those which are consistent with the electron diffraction patterns, i.e., $(h + k)$ even and strong reflections only in the neighborhood

TABLE II

X-RAY POWDER DATA FOR $Nb_2O_5 \cdot 11WO_3$

d (Å)[a]	$1/d^2_{obs}$	$h\,k\,l$	$1/d^2_{calc}$	I^a	F^b_{obs}	F^b_{calc}
4.638	0.0465	22 0 0	0.0454	5	47	−38
4.308	0.0539	24 0 0	0.0540	7	60	58
3.966	0.0636	26 0 0	0.0634	25	122	−117
3.850	0.0675	0 0 1	0.0674	350	472	471
3.726	0.0720	1 1 0	0.0720	230	280	314
3.690	0.0734	28 0 0	0.0735	350	494	−454
3.116*B*	0.1030			15		
2.764*B*	0.1309	25 1 0 26 0 1	0.1305 0.1308	10		65 −96
2.677	0.1395	1 1 1	0.1394	178	250	247
2.670	0.1403	27 1 0 28 0 1	0.1403 0.1409	190		−315 −354
2.579	0.1504	29 1 0	0.1508	28	146	−165
2.202	0.2062			25		
2.190	0.2085	27 1 1	0.2077	25	118	−245
2.139	0.2186	29 1 1	0.2182	12	84	−132
1.998*B*	0.2505			10		
1.927	0.2693	0 0 2	0.2696	90	518	481
1.910	0.2741	54 0 0	0.2735	30	304	228
1.865	0.2875	0 2 0	0.2876	58	434	475
1.845	0.2938	56 0 0	0.2942	90	547	390
1.812*B*	0.3046			18		
1.712	0.3412	24 2 0 54 0 1 1 1 2	0.3416 0.3409 0.3416	32		50 192 266
1.700	0.3460			14		
1.677	0.3556	55 1 0 0 2 1	0.3556 0.3550	100		382 395
1.664	0.3612	28 2 0 56 0 1	0.3611 0.3616	50		−380 326
1.569	0.4062			8		
1.541	0.4211	55 1 1 29 1 2	0.4230 0.4204	18		316 −149
1.530	0.4272	28 2 1	0.4285	25	256	−315
1.493*B*	0.4486			10		

B—broad.

[a] data from Roth and Waring (*9*), I = intensity.

[b] structure factors (F) are on an arbitrary scale.

of the sublattice spots, for which h has values around 0, 28, 56, etc. Most of the remaining unindexed lines were described as broad by Roth and Waring. A few of them could be fitted either by doubling the c axis, as indicated by Fig. 1a, or by altering the value of n from 14 to 15 or 16.

The $(410)_R$ patterns (e.g., Fig. 1c) were rather more streaked than the $(100)_R$ patterns. The 13 best patterns were measured carefully, and the subdivision of the reciprocal lattice between the 000 and 140 subcell spots lay between 54 and 63. Some of the patterns contained evidence for several sets of superlattice spots. Approximate unit cell dimensions for a monoclinic 60-fold supercell were

$$a = 15.5 \text{ Å}, \quad b = 3.83 \text{ Å},$$
$$c = 54.2 \text{ Å}, \quad \beta = 94.5°$$

Attempts to index Roth and Waring's powder data for $Nb_2O_5 \cdot 15WO_3$ on the basis of this supercell were unsuccessful. All the observed data were fitted by a large number of combinations of h, k, and l, but the criterion that strong reflections should occur only in the neighborhood of sublattice spots was not satisfactorily met. Since the electron diffraction patterns indicated the presence of a number of different superlattices, it is not surprising that the X-ray data were not fitted by a single set of lattice parameters.

The $(210)_R$ patterns were always heavily streaked, and therefore were not analyzed in detail. Fragments of this material would give diffuse X-ray patterns containing a few strong subcell reflections, which would probably overlap with those of the $(100)_R$ and $(410)_R$ patterns and of the various forms of WO_3. This is the probable reason why this component was not identified in the mixtures previously.

3.2 Electron Microscopy

Electron micrographs were recorded from fragments whose orientations were close to those indicated by the diffraction patterns in Fig. 1. Enhanced contrast was obtained by tilting a few degrees away from the zone axis orientation. All the images contained dark lines which lay predominantly in a direction perpendicular to the observed streaking in the diffraction patterns. Figure 2 shows

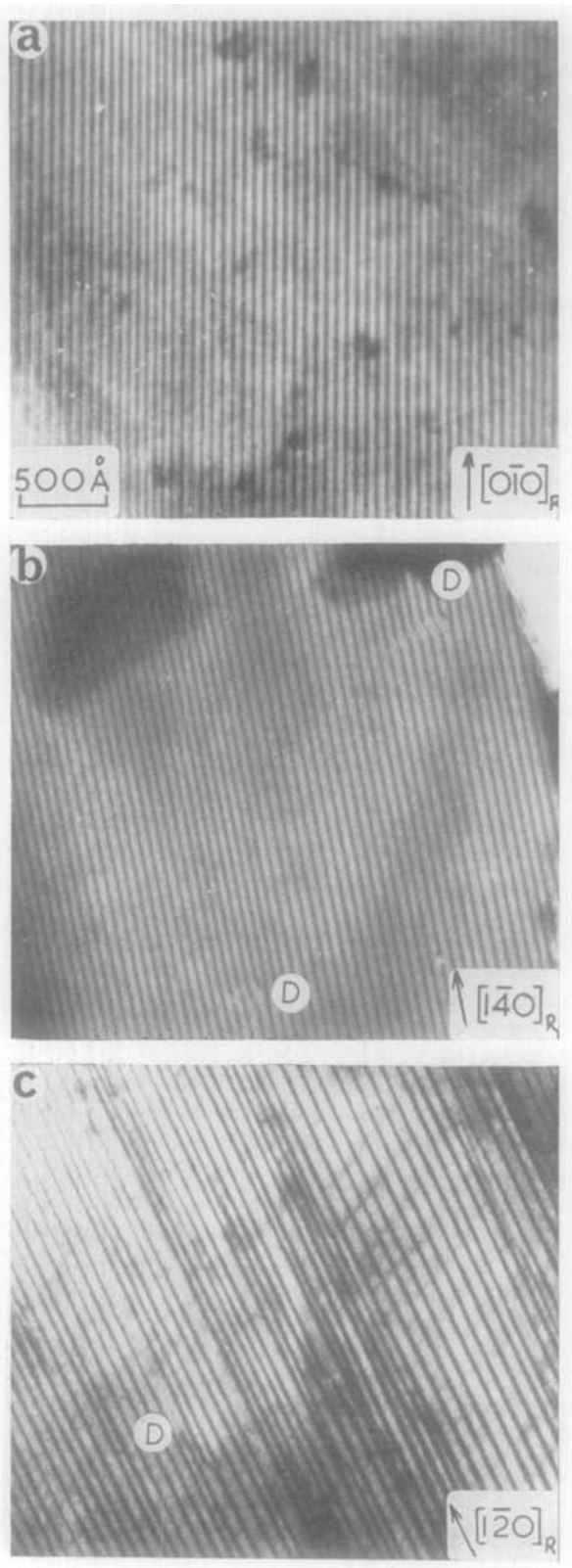

FIG. 2. Electron micrographs from fragments of nominal composition $Nb_2O_5 : WO_3 = 1:11$ (a) and 1:15 (b, c), showing straight dark lines. The orientation of the fragments in (a), (b), and (c) was similar to those shown by the diffraction patterns in Fig. 1b, c, and d, respectively. The direction of the lines with respect to the ReO_3-type subcell is shown. Several lines in (b) and (c) terminate within the fragments near D. The magnification mark in (a) applies to all three micrographs.

examples where most of the lines are straight, and lie along $[0\bar{1}0]_R$ in (a), $[1\bar{4}0]_R$ in (b), and $[1\bar{2}0]_R$ in (c). They were chosen to exhibit the most regularly spaced sequences of lines which were observed. In Fig. 2a, the lines have a spacing of 55 Å, which corresponds within experimental error with the spacing of (200) planes derived from the diffraction data for $Nb_2O_5 \cdot 11WO_3$ (51.7 Å for $n = 14$, 55 Å for $n = 15$). The spacings in Fig. 2b are rather less regular, ranging from about 48 Å to 60 Å, as expected from the spacings of superlattice spots in patterns like Fig. 1c. Several lines in Fig. 2b terminate within the fragment, and surrounding lines deviate near these terminations. In Fig. 2c, the spacings vary widely, from about 50 Å up to 120 Å. Several terminations are also evident in the regions marked D.

These observations are consistent with the diffraction patterns in Fig. 1. The increased streakiness of these patterns in the order $(100)_R$ (a, b), $(410)_R$ (c) and $(210)_R$ (d), is accompanied by increased irregularity of the spacing of the lines in the corresponding images, Figs. 2a, b and c, respectively.

Many of the fragments showed much more complex arrangements of lines than is indicated by Fig. 2. In particular, the lines were often wavy rather than straight, as shown in Fig. 3. Figures 3b and c were recorded from the same area of a crystal, but with slightly different orientations. In both cases, the crystal was tilted a few degrees away from the zone axis, but the tilt axis was approximately perpendicular and parallel to the majority of the lines in (b) and (c), respectively. The width of the lines is much greater in (c) than in (b) especially in thicker parts of the crystal away from its edge *E*. This indicates that the lines are the projections of surfaces within the crystal which lie parallel to a

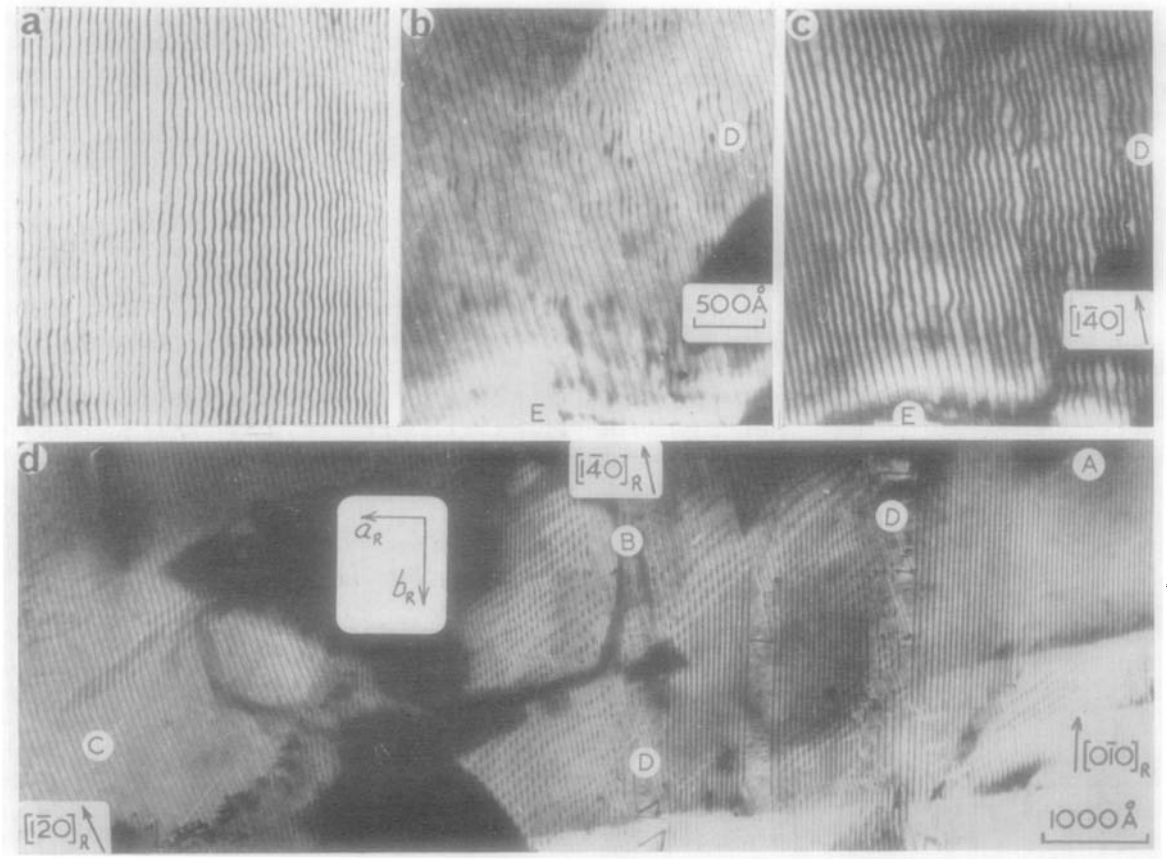

FIG. 3. Electron micrographs of fragments of nominal composition $Nb_2O_5:WO_3 = 1:11$ heated at 1623°K for 17 hr, showing wavy dark lines. The orientation of the ReO_3-type subcell, shown in (d), is the same for all the micrographs, and (a–c) have the same magnification, indicated in (b). (b) and (c) show two images of the same area, but in (c) the fragment was tilted a few degrees about $[1\bar{4}0]_R$. The edge of the fragment is marked *E*. Some of the lines terminate within the fragments, e.g., near *D* in (b–d).

short (= 3.8 Å) axis. When the lines are straight, these surfaces are planes, parallel to $(100)_R$, $(410)_R$, and $(210)_R$, as indicated by the diffraction patterns in Fig. 1. Nonplanar surfaces which appear as wavy lines in Fig. 3 were common. In Figs. 2b and 3b and d, the lines vary in width when their direction changes slightly. This is because the crystals are tilted slightly, and only those parts of the surfaces which lie perpendicular to the tilt axis appear as thin lines in projection. Others project as thick or even double lines according to their angle to the tilt axis.

The micrograph in Fig. 3d contains regions marked A, B, and C in which the direction of the black lines is predominantly parallel to $[0\bar{1}0]_R$, $[1\bar{4}0]_R$, and $[1\bar{2}0]_R$, respectively. Only the $[0\bar{1}0]_R$ lines are straight and regularly spaced over any appreciable area; the remainder, particularly those parallel to $[1\bar{4}0]_R$, contain many waves or "steps." Several lines labelled D contain very sharp bends, and terminate within the fragment.

4. Discussion

4.1. Possible Structures for $Nb_2O_5 \cdot xWO_3$

The present electron optical observations support Roth and Waring's (*9*) conclusion from X-ray powder data that the structures of WO_3 containing 6–9 mole% of Nb_2O_5 are related to those of the "Magnéli phases" (*11*), which all contain crystallographic shear planes (or "recurrent dislocations of atoms" in Magnéli's early papers.)

Let us consider first the simple cases where the lines in the micrographs are straight, indicating the presence of planar discontinuities in the structures, lying parallel to $(100)_R$, $(410)_R$, and $(210)_R$ planes of the pseudocubic WO_3 matrix as indicated in Figs. 1 and 2. The appearance of both the diffraction patterns and the micrographs is very similar to those of WO_{3-x} ($x \leqslant 0.05$) (*5, 6, 8*), and it is therefore probable that the discontinuities are crystallographic shear planes. However, in WO_{3-x}, these planes lie parallel to $\{210\}_R$ for $x \simeq 0.01$ (*5, 8*) and to $\{310\}_R$ for $x \simeq 0.05$ (*6*). Andersson (*12*) found CS planes parallel to $(100)_R$ in the oxide fluoride Nb_3O_7F, and discussed the structural principles of a homologous series M_nO_{3n-1} containing CS planes in this direction, and varying only in spacing. CS planes parallel to $(410)_R$ have not been reported previously, but nevertheless, Magnéli (*11*) has analyzed the geometrical characteristics of hypothetical structures of this kind, and his formulae can be used to derive idealized unit cell dimensions of ordered structures containing CS planes in this direction.

Let us now propose idealized structures for the observed phases, and derive their unit cell dimensions and compositions.

(*a*) *CS Parallel to* $(100)_R$. Figure 4a shows the idealized structure of $M_{14}O_{41}$, containing CS planes parallel to $(100)_R$, and based on Andersson's determination of the structure of Nb_3O_7F (*12*). It is orthorhombic, space group *Cmmm*, with

$$a = (2n - 1) \times 3.8 \text{ Å} = 103 \text{ Å for } n = 14,$$
$$b = c = 3.8 \text{ Å},$$

where 3.8 Å is the distance between metal atoms in the ideal ReO_3-type sublattice. These dimensions are to be compared with $a = 103.3$ Å, $b = 3.729$ Å, $c = 3.852$ Å, derived from the X-ray powder data (Table II).

The composition of the idealized structure with $n = 14$ is $M_{14}O_{41}$ ($MO_{2.929}$), and this is fitted in the Nb_2O_5–WO_3 system by $Nb_2O_5 \cdot 12WO_3$, which is in fair agreement with the composition $Nb_2O_5 \cdot 11WO_3$ proposed by Roth and Waring (*9*). It was noted in the present work that as the composition tended towards pure WO_3, higher homologues ($n = 15, 16$) of the same series of phases [CS parallel to $(100)_R$] were observed. Their compositions $M_{15}O_{44}$ ($MO_{2.933}$) and $M_{16}O_{47}$ ($MO_{2.938}$) also tend towards MO_3.

An attempt was made to obtain additional confirmation of the proposed structure by calculating structure factors and comparing these with those derived from the X-ray powder data, suitably corrected for multiplicity and Lorenz and polarization effects. This comparison was confined initially to the *h*00 reflections, and the results are shown in Fig. 5. Figure 5a represents the values of $|F_{obs}|$ for the six observed *h*00 reflections ($h = 22, 24, 26, 28, 54, 56$). Figure 5b shows calculated values of $|F_c|$ for $h = 20$–60, for the idealized structure in Fig. 4a. The scattering curve for W^{6+} was modified slightly to allow for the presence of a random distribution of Nb^{5+}. The most obvious feature of Fig. 5b is that the strong reflections occur in very restricted groups around $h = 26$–28, and $h = 54$. This is consistent with the electron diffraction patterns (Figs. 1a, b), and also with Fig. 5a, but the agreement in detail between Figs. 5a and 5b is poor. In particular, the calculated values of F_c for $h = 26$ and 54 are too high, and those for $h = 28$ and 56 are too low. Hence, the idealized structure requires modification, and the most obvious way of doing this is to introduce a distortion in the vicinity of the shear planes. Andersson (*12*) found that for Nb_3O_7F, the metal atoms in the octahedra which share edges were pushed away from their ideal

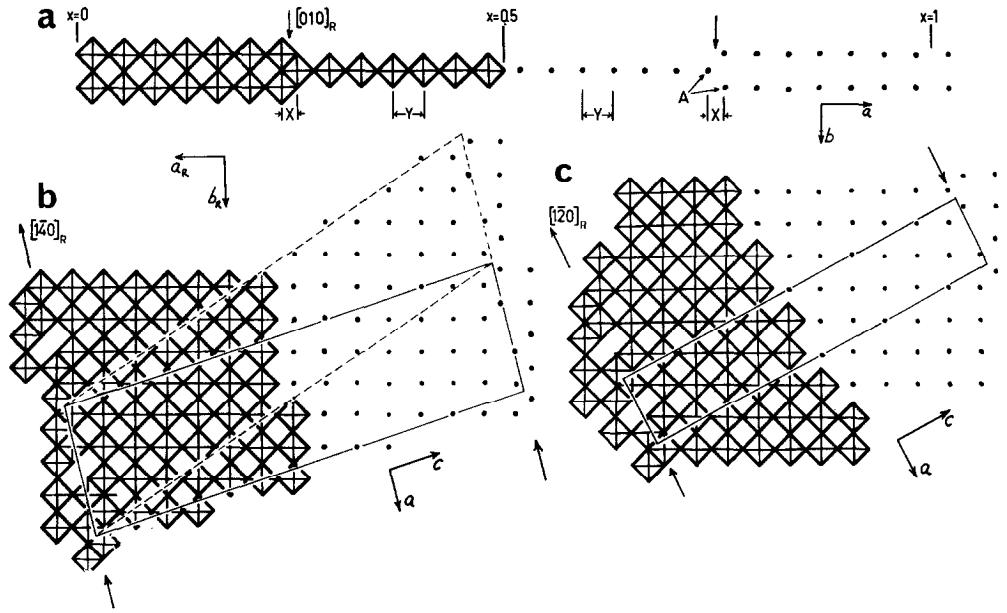

FIG. 4. Idealized drawings of possible structures of (a) $M_{14}O_{41}$ containing CS planes parallel to $(100)_R$, (b) $M_{60}O_{177}$ containing CS planes parallel to $(410)_R$, (c) $M_{27}O_{80}$, containing CS planes parallel to $(210)_R$. Each square represents an MO_6 octahedron, viewed down a body diagonal, and on the right of each model, only the positions of metal ions are shown. The axes a_R and b_R refer to the ReO_3-type subcell, and the true unit cells are outlined in (b) and (c). The CS planes are marked by arrows.

positions, such that the distance X in Fig. 4 was 2.73 Å, 44% greater than the ideal 1.9 Å ($=\frac{1}{2}Y$ in Fig. 4). Magnéli (*11*) found a similar distortion for the reduced tungsten and tungsten–molybdenum oxides, and included this effect in his treatment of hypothetical shear structures. A series of calculations was carried out with increasing values of X until best fit with the six observed $h00$ data was obtained. This is shown in Fig. 5c, for which $X = 3.08$ Å, $Y = 3.74$ Å, and the reliability factor,

$$R_{h00} = \sum (|F_{calc}| - |F_{obs}|) \times 100/\sum |F_{calc}|$$

was 12%. This value of X is considerably higher than was obtained for other structures of this kind (*11*, *12*), but this is not surprising because we have chosen to alter one of many possible parameters.

A second modification which can be easily tested is to assume that the four niobium atoms in the unit cell are not randomly distributed on the cation sites, but lie in one of the fourfold positions of the space group *Cmmm*. The only fourfold position which differs significantly from others in the structure is that marked A in Fig. 4a. All the metal atoms lying in octahedra which shares edges belong to this fourfold group. A further series of calculations with niobium ordered in these sites also gave best correspondence for $X = 3.08$ Å, $Y = 3.74$ Å (Fig. 5d), and the reliability factor R_{h00} improved to 9%.

No further attempts to improve on this model were made. When applied to all the *hkl* reflections for which independent measurements of intensity were available, the over-all reliability factor was 16%, and was not significantly different for random or ordered occupancy of the metal sites. The calculated intensities for the ordered model with $X = 3.08$ Å are included in Table I. The correspondence with the observed data may be considered reasonable, in view of the simplicity of the structural model. In particular, the electron diffraction evidence for a doubling of the c axis (Fig. 1a) has been completely ignored. It seems likely that, as in the case of WO_3 (*13*), the doubling is caused by a puckering of the layers of metal atoms about the (001) planes.

(*b*) *CS Parallel to* $(410)_R$. Figure 4b shows an idealized structure for $M_{60}O_{177}$, containing shear planes parallel to $(410)_R$. This model is based on Magnéli's general discussion of shear structures (*11*), and using his formulae (which include the effects of distortion near the shear planes), the following dimensions for the monoclinic unit cell (space group $P2/m$) were obtained:

$$a = 15.5 \text{ Å}, \quad b = 3.75 \text{ Å},$$
$$c = 57.3 \text{ Å}, \quad \beta = 70°14'$$

This unit cell is dotted in Fig. 4b. A more appropriate unit cell, with β closer to 90°, is marked with full lines in Fig. 4b. Its calculated dimensions are:

$$a = 15.5 \text{ Å}, \quad b = 3.75 \text{ Å},$$
$$c = 54.1 \text{ Å}, \quad \beta = 94° 7'$$

These dimensions compare favorably with those of a 60-fold supercell measured from electron diffraction patterns, i.e.,

$$a = 15.5 \text{ Å}, \quad b = 3.83 \text{ Å},$$
$$c = 54.2 \text{ Å}, \quad \beta = 94° 30'$$

The composition of this structure is $M_{60}O_{177}$, or $Nb_2O_5 \cdot 18WO_3$. Other members of this series M_nO_{3n-3}, with $n = 54$–63 found by electron diffraction, correspond to compositions between $Nb_2O_5 \cdot 16WO_3$ and $Nb_2O_5 \cdot 19WO_3$. These compositions are all slightly deficient in Nb_2O_5 by comparison with Roth and Waring's estimate of $Nb_2O_5 \cdot 15WO_3$ for this phase.

Because the X-ray powder diffraction pattern of $Nb_2O_5 \cdot 15WO_3$ was not satisfactorily indexed, no further confirmation of the proposed structure could be obtained from a comparison of observed and calculated structure factors. However, the appearance of the electron diffraction patterns is consistent with a structure consisting of extended slabs of an ReO_3-type lattice containing periodic discontinuities parallel to $(410)_R$. The discontinuities are presumed to be CS planes, as shown in Fig. 4b.

(*c*) *CS Parallel to* $(210)_R$. Electron diffraction patterns (Fig. 1d) and transmission micrographs (Fig. 2c) from fragments containing CS planes parallel to $(210)_R$ both indicated that the arrangement of these planes was much more irregular than was the case for CS parallel to $(100)_R$ and $(410)_R$. In this respect, the results are similar to those for WO_{3-x} ($x \leqslant 0.01$), where randomly spaced arrays of CS planes parallel to $(210)_R$ were frequently observed (*5*, *8*). Nevertheless, it is possible to propose a structure for these shear planes, and to make a rough estimate of the composition of individual fragments. Figure 4c shows an idealized model of $M_{27}O_{80}$, containing CS planes parallel to $(210)_R$ (arrowed), whose geometry is assumed to be similar to those found in the reduced molybdenum–tungsten mixed oxides, $(Mo,W)_nO_{3n-1}$ (*14*). It has been shown previously (*8*) that the spacing of $\{210\}_R$ CS planes in the series M_nO_{3n-1} is given by $S \simeq 0.85(2n-1)$ Å. This formula may be used to derive the average value of n for a fragment containing irregularly spaced CS planes, if the average spacing is known and it is assumed that all the CS planes have the same area.

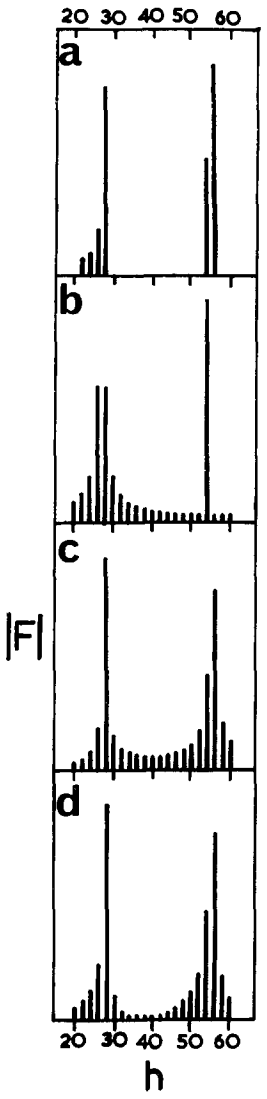

FIG. 5. Structure factors $|F|$ relating to proposed models of $Nb_2O_5 \cdot 12WO_3$. (a) Observed $h00$ data, after Roth and Waring (*9*). (b–d) Calculated data, for the model shown in Fig. 4a. (b) $X = \frac{1}{2}$ $Y = 1.9$ Å, W and Nb disordered. (c) $X = 3.08$ Å, $Y = 3.74$ Å, W and Nb disordered. (d) $X = 3.08$ Å, $Y = 3.74$ Å, Nb ordered in CS planes (A in Fig. 4a).

For example, in Fig. 2c, the average spacing of the dark lines is 70 Å, which according to the equation above, corresponds to $n \approx 40$. The calculated average composition is therefore $M_{40}O_{119}$, or $Nb_2O_5 \cdot 38WO_3$. A survey of a number of micrographs of fragments containing CS planes parallel to $\{210\}_R$ indicated that their average compositions tended towards MO_3 as the Nb_2O_5 content was reduced, but was always closer to MO_3 than the nominal composition of the samples.

4.2 Solid Solution of Nb_2O_5 in WO_3

Roth and Waring (*9*) noted that WO_3 could accept up to 3 mole% of Nb_2O_5 into solid solution, and that the presence of niobium stabilized the high temperature forms of WO_3. This conclusion has not been specifically investigated in the present work, but the results indicate that it is probably substantially correct. The presence of fragments containing CS planes parallel to $\{210\}_R$ in the 1:32.3 sample (Table I) suggests that the extent of solid solution is less than 3 mole% Nb_2O_5. However, the number of fragments of this type, and the numbers of CS planes within them was certainly insufficient to account for an over-all $Nb_2O_5:WO_3$ ratio of 1:32.3 without a significant contribution from solid solution.

The small discrepancies between the compositions of the "Magnéli phases", as determined by Roth and Waring (*9*), and those of their idealized structures postulated in this paper, might well be due to the presence of additional Nb_2O_5 in solid solution. For example, if 1 mole% of Nb_2O_5 was incorporated in the structures Figs. 4a, b as solid solution, their compositions would be

$$Nb_2O_5:12(0.01Nb_2O_5:0.99WO_3) = Nb_2O_5:10.6WO_3. \quad \text{(Fig. 4a)}$$

and

$$Nb_2O_5:18(0.01Nb_2O_5:0.99WO_3) = Nb_2O_5:15.1WO_3. \quad \text{(Fig. 4b)}$$

These modified compositions approach those derived by Roth and Waring ($Nb_2O_5:11WO_3$ and $Nb_2O_5:15WO_3$) very closely.

No information concerning the nature of these solid solutions was obtained from the electron optical observations. The composition may be adjusted either by removing oxygen ions or by inserting additional metal ions. The structures of all these ReO_3-type phases are very open, and therefore the latter alternative seems most likely.

4.3 NonPlanar CS Surfaces

The micrographs in Fig. 3 provide evidence for nonplanar discontinuities which may be referred to as CS surfaces. They frequently occur together with CS planes in the same fragment (e.g., Fig. 3d) and they probably have a similar origin and structure. In Figs. 3a and b the "average" direction of the shear planes, as indicated by the corresponding diffraction patterns is $[0\bar{1}0]_R$ and $[1\bar{4}0]_R$, respectively. Deviations from these general directions are common, and a consideration of the idealized structures in Fig. 4 indicates that models of CS surfaces can be derived readily. The CS planes all contain groups of edge-shared octahedra of the form shown in Fig. 6a. In $\{100\}_R$ CS planes, these groups are of continuous extent along the *a* axis. For any CS plane parallel to $\{m10\}_R$, the groups will contain $2m$ octahedra joined by sharing edges. There is no structural reason why successive groups along a CS surface should be of the same size. Only when the groups *are* of the same size will the CS surface be a plane. Fig. 6b shows an arrangement of metal atoms in a $(001)_R$ plane which is traversed by several CS surfaces containing bends similar to those seen in Fig. 3. The groups of metal atoms which lie in edge-shared octahedra are outlined. From a geometrical point of view, any CS surface of this kind fits into the ReO_3-type matrix as easily as a simple CS plane even when the CS surface suffers a sharp change of direction, as at D in Figs. 3d, 6b.

4.4 Equilibrium Structures

In principle, it would be possible to cover the whole range of compositions studied by means of a single series of phases, say M_nO_{3n-1}, in which the spacings of CS planes steadily decreased as the Nb_2O_5 content increased. In practice, the situation is clearly much more complicated than this. Not only are several different series of phases involved, but in addition, CS surfaces have been observed as well as planes. Some of these effects are undoubtedly due to the fact that equilibrium has not been attained in any of the samples. In particular, it seems probable that CS surfaces will tend to become planar after long annealing, and that these planes will move laterally until they are regularly spaced. On a microscopic scale, these conditions are approached much more closely in the fragments shown in Fig. 2 than in those shown in Fig. 3. The driving force for both these processes is probably very small indeed, especially when the CS surfaces are widely separated, hence equilibrium is likely to be very difficult to achieve.

The presence of three different series of phases, covering different composition intervals and having CS planes parallel to $(100)_R$, $(410)_R$, and $(210)_R$ is probably a real effect, not associated with departures from equilibrium. This observation can be explained if one assumes that the free energy of the system is influenced more by the *spacing* of CS planes than by their *orientation*. In nearly all the fragments examined by electron microscopy, the spacing of CS planes lay between 50 and 70 Å. The consequent effect on the composition of the fragments depends upon the direction of the CS planes. Relevant data, derived from a consideration of the geometry and

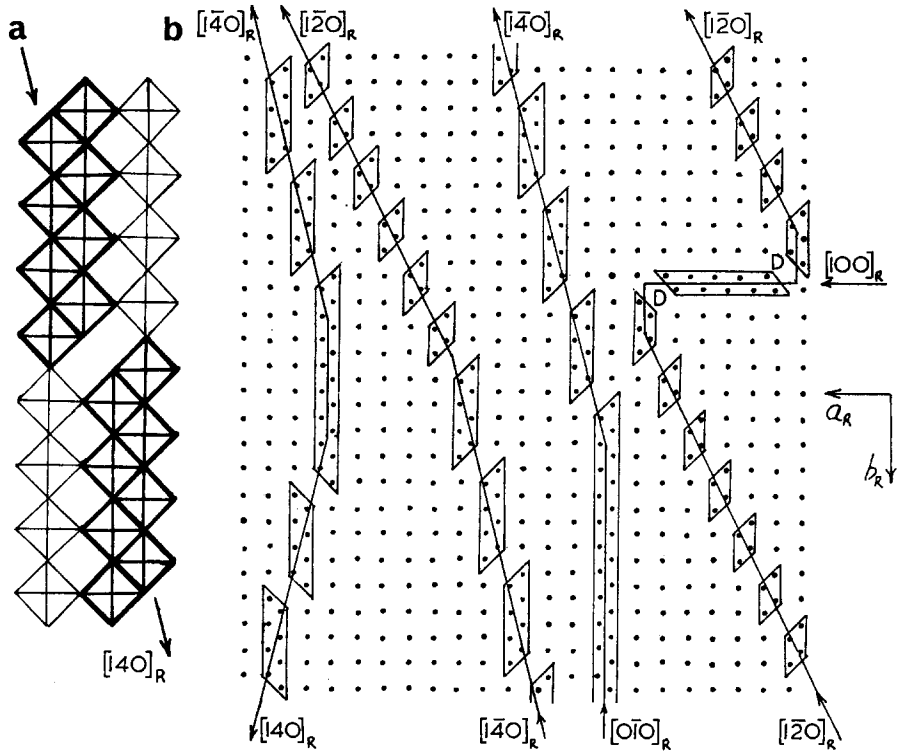

FIG. 6. (a). Two groups of eight edge-shared octahedra (in heavy outline) forming part of a CS plane parallel to $(410)_R$. (b) Model showing the arrangement of metal ions in a $(001)_R$ plane, traversed by CS surfaces in a variety of directions, corresponding to some of those observed in Fig. 3. Atoms which lie in groups of edge-shared octahedra are outlined.

the contents of the unit cells of structures such as those shown in Fig. 4, are recorded in Table III. For the range of spacings 50–70 Å, the compositions between O/M = 2.93 (i.e., $Nb_2O_5 \cdot 12WO_3$) and O/M = 2.98 ($Nb_2O_5 \cdot 50WO_3$) are covered almost completely by three series of phases with CS planes parallel to $\{100\}_R$, $\{410\}_R$, and $\{210\}_R$. The compositions obtained using $\{310\}_R$ overlap with the $\{410\}_R$ and $\{210\}_R$ cases. Groups of CS planes parallel to $\{310\}_R$ were not observed in this study, although micrographs such as Fig. 3d contain short segments of CS surfaces which probably lie in this direction. It is an interesting possibility that careful control of annealing conditions, together with long periods of time, might reduce the range of energetically favored CS plane spacings and lead to the formation of a $\{310\}_R$ series in the Nb_2O_5–WO_3 system.

TABLE III

RELATION BETWEEN DIRECTION OF CS PLANES AND COMPOSITION

Direction of CS plane	Formula of series[a]	Spacing of CS planes, S[a]	Value of n for S = 50 Å	Value of n for S = 70 Å	Range of Composition O/M
$\{100\}_R$	M_nO_{3n-1}	$(n-\frac{1}{2})a$	14	19	2.929–2.947
$\{410\}_R$	M_nO_{3n-3}	$(n-1\frac{1}{2})a/\sqrt{17}$	56	77	2.946–2.961
$\{310\}_R$	M_nO_{3n-2}	$(n-1)a/\sqrt{10}$	43	59	2.953–2.966
$\{210\}_R$	M_nO_{3n-1}	$(n-\frac{1}{2})a/\sqrt{5}$	30	42	2.967–2.976
$\{110\}_R$[b]	M_nO_{3n}				3.000 fixed

[a] The general formula for a series with CS planes parallel to $\{m10\}_R$ ($m \neq 0$) is M_nO_{3n-m+1}. The spacing of CS planes is given by $S = [(2n - m + 1)/2\sqrt{1 + m^2}]a$, where a is the distance between metal atoms in the ReO_3-type subcell. a = 3.8 Å.

[b] CS planes parallel to $\{110\}_R$ do not alter the composition (*8*).

When the present results are compared with those for other similar systems, systematic trends are difficult to detect. For example, WO_{3-x} exhibits CS parallel to $\{210\}_R$ for $x < 0.02$ (*5*, *8*) and $\{310\}_R$ for $x \simeq 0.05$ (*6*), the spacings in the latter case, [i.e., $W_{20}O_{58}$, (*7*)] being 23 Å, considerably less than any of the spacings observed in $Nb_2O_5 \cdot 11$–$32\ WO_3$. On the other hand, in the $(Mo,W)O_{3-x}$ system, CS parallel to $\{210\}_R$ persists down to $x = 0.125$ (i.e., Mo_8O_{23}, *15*), and spacings as small as 13 Å are observed. Several series of phases occur also in TiO_{2-x} (*16*) with CS planes parallel to {132} for $x \lesssim 0.07$ and parallel to {121} at $x = 0.11$–0.25. In each of these systems, the differences in energy between various possible phases are likely to be small, and there is probably a sensitive balance between the stability of a particular phase, the composition, the temperature, and the partial pressure of oxygen.

Table III shows clearly that within the $\{m10\}_R$ series of phases, CS planes parallel to $\{210\}_R$ have the least possible effect on stoichiometry. This is in accord with the experiment, since both here and in an earlier study of WO_{3-x} (*8*) samples for which O/M lay close to 3.0 contained CS planes in this direction only. There appears to be no alternative plane (*hkl*) for CS at very small departures from the MO_3 composition, since even in $WO_{\leqslant 2.994}$, $\{210\}_R$ CS planes were observed, irregularly arranged with average spacings of $\gtrsim 300$ Å (*8*). In these circumstances, the interaction energy between neighboring CS planes must be vanishingly small, and ordering processes will be extremely slow. The lowest energy configuration might well involve groups of closely spaced (say 50 Å) CS planes surrounded by defect-free regions of WO_3, rather than regularly arranged CS planes spaced hundreds of Å apart.

4.5 Formation and Movement of CS Surfaces

The initial formation and subsequent diffusive movement of CS surfaces has occupied the attention of a number of groups of workers. Several mechanisms have been proposed (*17*–*19*) and the results of recent relevant electron optical studies have been discussed in terms of these. The over-all conclusion is that Anderson and Hyde's dislocation mechanism (*18*) for the formation of CS planes has considerable merit, and that Andersson and Wadsley's cooperative diffusion approach (*19*) is more appropriate for describing the lateral motion of CS planes, which must occur during ordering processes (*6*, *16*, *20*, *21*).

Several examples of CS surfaces terminating within a fragment, presumably at dislocations, are apparent in Figs. 2b and 3b, d. Tilley (*8*) has proposed models for such terminations, and suggested a detailed mechanism for the formation of CS planes in WO_{3-x}, involving their nucleation at a surface followed by extension into the bulk by preferential loss of oxygen from the vicinity of the terminating dislocation. He also showed that CS planes parallel to $\{210\}_R$ would be preferred over other orientations at small values of x. A similar mechanism might apply to the case where loss of oxygen is replaced by diffusion of Nb^{5+} into the WO_3 lattice. The terminating dislocation could act as a sink for migrating Nb^{5+} cations, which would then be "built in" to the growing CS surface.

It remains to discuss how the CS surfaces once formed can become planar, and move laterally into an ordered sequence. Andersson and Wadsley's approach to the problem (*19*) requires some modification, since they did not recognize the possibility that nonplanar CS surfaces could exist. This led them to suggest that large numbers of ions could move cooperatively in order that a CS plane could move laterally *as a plane* through the crystal. However, the observation of CS surfaces (e.g., Fig. 3) and also of displacements and steps in CS planes (*22*) suggests that this cooperative motion can be broken up into discrete diffusive processes involving only a few ions at any one instant.

Let us consider, for example, how a CS surface might become planar. Figure 7a shows a junction between two groups of octahedra, similar to those which occur in all the CS surfaces in Figs. 4 and 6. The arrow marks a possible movement of a metal ion, together with the oxygen ions which lie above and below it along the c_R axis (i.e., perpendicular to the plane of the paper). The consequence of such a movement, shown in Fig. 7b, is to shift the junction along the shear plane. This process can occur in successive unit cells or layers of octahedra in the c_R direction. The structures shown in Figs. 7a and b can be placed one on top of the other in a coherent fashion, forming three dimensional model of a "kink" in the junction. The passage of such a kink through the crystal leads finally to a shift of the junction along the shear plane.

Figure 7c shows a sequence of motions of the type shown in Fig. 7a, b, applied to a CS surface containing segments parallel to $(100)_R$ and $(410)_R$. Only the metal atoms are shown. The final result of the sequence is to produce a continuous $(410)_R$ CS plane. Figure 7d shows how a $(100)_R$ CS plane can move laterally, by the propagation of a junction (circled) along it.

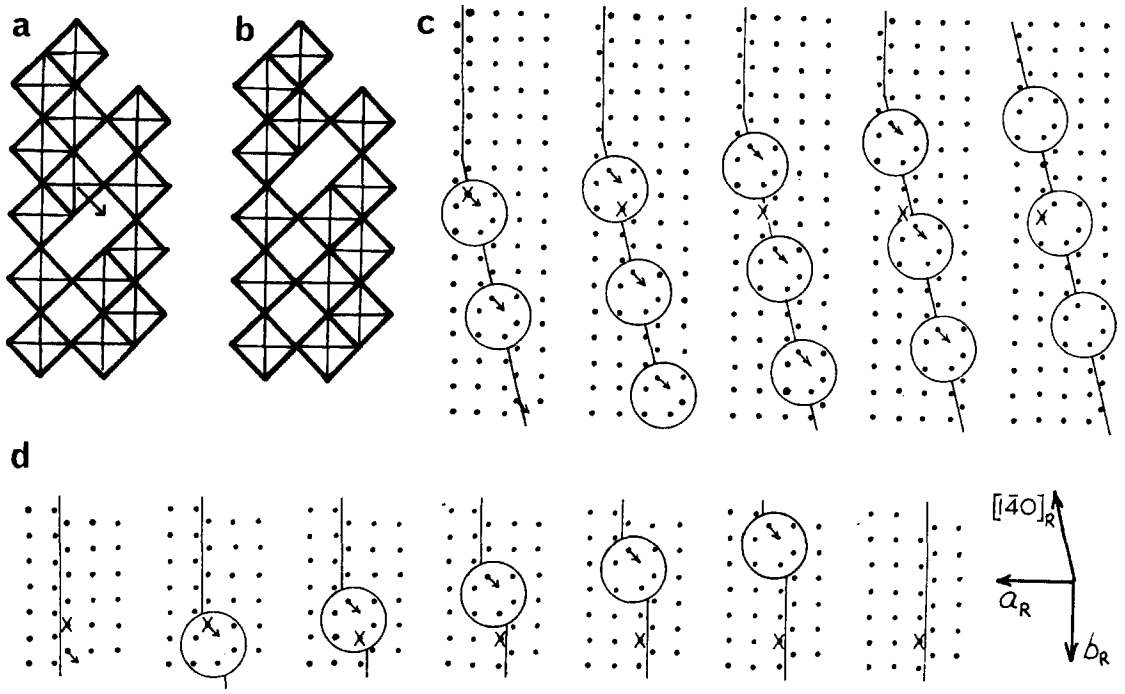

FIG. 7. (a–b) Part of a CS plane, showing how the movement of a metal ion and two of its neighbor oxygen ions (above and below the plane of the paper) in the direction marked by the arrow in (a), results in a movement of the junction between two groups of edge-shared octahedra. (c) Sequence of movements of the type detailed in (a), applied to a CS surface containing segments parallel to $(100)_R$ and $(410)_R$. The end result is to produce a continuous $(410)_R$ CS plane. (d) Sequence of movements showing how a $(100)_R$ CS plane might diffuse laterally, by the propagation of a junction along it. In (c) and (d), only the metal ions are shown, and junctions between groups of edge-shared octahedra in the CS surfaces are circled. Individual ions move only once during each sequence, as shown by reference to those marked with a cross.

It is important to notice that this mechanism does not allow for any major redistribution of metal atoms. For example, the atoms marked by a cross in Figs. 7c, d move only once during the sequence of events. This implies that the movement of CS surfaces is not the means by which, in this instance, the Nb^{5+} ions are distributed through the WO_3 matrix. From this point of view, the process is fundamentally different from that of the formation of WO_{3-x} by reduction, where a uniform distribution of W^{5+} ions can be achieved merely by electron exchange. Andersson (*23*) arrived at a similar conclusion following his study of the reaction of Nb_2O_5 with MoO_3 vapor. He showed that the structural rearrangements which accompany the reaction could be achieved by small displacements of relatively few atoms, and he suggested that the associated long-range migration of Mo^{6+} ions was a separate process, involving interstitial diffusion parallel to the [010] direction in Nb_2O_5.

From the point of view of diffusion, the arrangement of CS surfaces in the fragment shown in Fig. 3d is particularly interesting, and warrants further discussion.

Using the data in Table III, it is easy to show that the compositions of the regions labelled A, B, and C should be approximately $Nb_2O_5 \cdot WO_3 = 1:12, 1:21$, and 1:41, respectively. It is tempting to conclude that this composition gradient across the fragment is a consequence of conditions prevailing during the original reaction. One possible explanation for the gradient is that during the reaction, the fragment was part of a larger crystal, and that the region A was closer to the source of diffusing Nb than the remainder of the fragment. If this were the case, CS surfaces would tend to form first in the region A, and it is apparent from their direction and spacing that the concentration of niobium in this region is close to the maximum which this phase can accommodate [i.e., $Nb_2O_5:WO_3 = 1:11$, according to Roth and Waring (*9*).] This is clearly a nonequilibrium situation, and equilibration must require the redistribution of CS surfaces, or the creation of new ones in B and C.

If additional niobium is still available from the source, there are several possible mechanisms for the subsequent appearance of CS surfaces to the left of A.

(a) Nucleation and growth of new CS surfaces in B and C. This requires diffusion of Nb ions into B and C, either through the existing CS surfaces in A, or via the exterior surface of the crystal, and then parallel to c_R. Because the CS surfaces contain closely packed octahedra, they should act as barriers to diffusing ions, hence the latter process of exterior surface migration is likely to be preferred. Several CS surfaces in B and C terminate within the crystal, which may indicate that they are growing *in situ* by this mechanism.

(b) Lateral migration of existing CS surfaces from A into B and C, via mechanisms of the type shown in Fig. 7. This process must be accompanied by diffusion of the Nb ions which are associated with each CS surface, but it does not involve diffusion *through* the CS surfaces. The supply of CS surfaces in A would be maintained by the creation of new ones adjacent to the source of Nb.

If we suppose that at the stage depicted in Fig. 3d, the source of Nb is depleted, then it appears that the migration of CS surfaces according to (b) above is the only process which could lead finally to a homogeneous distribution of Nb and a regular arrangement of CS planes over the entire fragment. Thus it seems certain that the migration of CS surfaces over relatively large distances is an important part of the reaction, particularly in the case where the initial reaction is confined to specific regions where the reactants happen to be in contact.

This is likely to be true for all reactions involving several solids, such as WO_3 with Nb_2O_5 or with W metal. The formation of WO_{3-x} by heating in a reducing atmosphere is not subject to the same constraints. It would, therefore, be of great interest to make a detailed comparison of the following three reactions:

(1) $WO_3 \rightarrow WO_{3-x}$ by heating in a reducing atmosphere.

(2) $WO_3 + W \rightarrow WO_{3-x}$ by heating in an inert atmosphere.

(3) $WO_3 + Nb_2O_5 \rightarrow (W,Nb)O_{3-x}$ by heating in air or oxygen.

In (1), reaction can proceed at all points on the surface of a WO_3 crystal, and the subsequent migration of CS surfaces does not involve any associated long range diffusion of ions, since a homogeneous distribution of W^{5+} can be achieved by electron transfer. Reaction (2) is similar, except that initial reaction should be restricted to areas of WO_3–W contact. Reaction (3) is initially restricted to areas of WO_3–Nb_2O_5 contact, and also requires long range diffusion of Nb^{5+} along with the migration of CS surfaces. Carefully controlled experiments of this kind will be necessary before we can arrive at more specific conclusions concerning the role of the various processes which must occur during the formation of phases containing CS planes.

Acknowledgment

I wish to thank Dr. J. V. Sanders for his continued interest in this work and for constructive comments.

References

1. G. Hagg and A. Magnéli, *Rev. Pure Appl. Chem.* **4**, 235 (1954).
2. A. D. Wadsley and S. Andersson *in* "Perspective in Structural Chemistry" (J. D. Dunitz and J. A. Ibers, eds.), Vol. III, Wiley, NY (1970).
3. J. G. Allpress, J. V. Sanders, and A. D. Wadsley, *Acta Crystallogr. Sect.* **B25**, 1156 (1969).
4. J. G. Allpress, *J. Solid State Chem.* **1**, 66 (1969).
5. R. J. D. Tilley, *Mater. Res. Bull.* **5**, 813 (1970).
6. J. G. Allpress and P. Gadó, *Crystal Lattice Defects* **1**, 331 (1970).
7. A. Magnéli, *Ark. Kemi* **1**, 513 (1950).
8. J. G. Allpress, R. J. D. Tilley, and M. J. Sienko, *J. Solid State Chem.* **3**, 440 (1971).
9. R. S. Roth and J. L. Waring, *J. Res. Nat. Bur. Stand.* **70A**, 281 (1966).
10. P. Gadó and A. Magnéli, *Mater. Res. Bull.* **1**, 33 (1966).
11. A. Magnéli, *Acta Crystallogr.* **6**, 495 (1953).
12. S. Andersson, *Acta Chem. Scand.* **18**, 2339 (1964).
13. B. O. Loopstra and P. Boldrini, *Acta Crystallogr.* **21**, 158 (1966).
14. B. Blomberg, L. Kihlborg, and A. Magnéli, *Ark. Kemi* **6**, 133 (1953).
15. A. Magnéli, *Acta Chem. Scand.* **2**, 501 (1948).
16. L. A. Bursill, B. G. Hyde, O. Terasaki, and D. Watanabe, *Phil. Mag.* **20**, 347 (1969).
17. P. Gadó, *Acta. Phys.* **18**, 111 (1965).
18. J. S. Anderson and B. G. Hyde, *J. Phys. Chem. Solids* **28**, 1393 (1967).
19. S. Andersson and A. D. Wadsley, *Nature* **211**, 581 (1966).
20. L. A. Bursill and B. G. Hyde *in* "The Chemistry of Extended Defects in Nonmetallic Solids" (L. Eyring and M. O'Keeffe, eds.), North Holland, Amsterdam (1970). (See also discussion of this paper.)
21. J. S. Anderson and R. J. D. Tilley, *J. Solid State Chem.* **2**, 472 (1970).
22. J. G. Allpress, *J. Solid State Chem.* **2**, 78, (1970).
23. S. Andersson, *Z. Anorg. Chem.* **366**, 96 (1969).